Cellulose (2018) 25:3471–3486
https://doi.org/10.1007/s10570-018-1791-6

ORIGINAL PAPER

Preparation, characterization, adsorption kinetics and thermodynamics of chitosan adsorbent grafted with a hyperbranched polymer designed for Cr(VI) removal

Qiaoping Li · Bin Xu · Linghua Zhuang · Xiaoqing Xu · Guowei Wang · Xinghua Zhang · Jing Chen · Yang Tang

Received: 15 November 2017 / Accepted: 10 April 2018 / Published online: 19 April 2018

Abstract Tetracarboxylic acid ester was synthesized with diethyl malonate and methyl acrylate, and an amino terminated hyperbranched polymer (HBP-NH_2) was prepared by reaction of a tetracarboxylic acid ester with diethylenetriamine (DETA). Hyperbranched polymer grafted chitosan (HBP-g-chitosan), a novel adsorbent material for Cr(VI) removal, was prepared from HBP-NH_2 and chitosan with epichlorohydrin as crosslinking agent. The adsorbent was characterized by thermogravimetric analysis, Fourier transform infrared spectroscopy, scanning electron microscopy, X-ray photoelectron spectrophotometry, and X-ray diffraction. The influence of the initial concentration of Cr(VI), the dosage of adsorbent, pH value and the coexisting anions on the adsorption performance were studied. An isotherm of the adsorption process was generated and studied by Langmuir and Freundlich models. The results showed that the Freundlich model proved to be more suitable than the Langmuir model. The adsorption kinetics were determined by pseudo-first order and pseudo-second order kinetics. In doing so, it was found that the pseudo-second order kinetic model was more reliable than the pseudo-first order kinetic model.

Keywords Chitosan · Hyperbranched polymer · Cr(VI) removal · Adsorption

Linghua Zhuang and Guowei Wang contributed equally to this work.

Electronic supplementary material The online version of this article (https://doi.org/10.1007/s10570-018-1791-6) contains supplementary material, which is available to authorized users.

Q. Li · B. Xu · G. Wang (✉) · X. Zhang · J. Chen · Y. Tang
College of Food Science and Light Industry, Nanjing Tech University, Nanjing 211800, Jiangsu, China
e-mail: kingwell2004@sina.com

G. Wang
Institute of Textile Chemicals and Ecological Dyeing and Finishing, Nanjing Tech University, Nanjing 211800, Jiangsu, China

L. Zhuang (✉)
College of Chemistry and Molecular Engineering, Nanjing Tech University, Nanjing 211800, Jiangsu, China
e-mail: zhuanglhnj@163.com

X. Xu
College of Biotechnology and Pharmaceutical Engineering, Nanjing Tech University, Nanjing 211800, Jiangsu, China

Abbreviations

BP-NH_2	Amino terminated hyperbranched polymer
XRD	X-ray diffraction
^{1}HNMR	H-Nuclear magnetic resonance
FT-IR	Fourier transform infrared spectroscopy
SEM	Scanning electron microscopy
TGA	Thermogravimetric analysis
XPS	X-ray photoelectron spectrophotometer
CrLHCh	Cr(VI) loaded to HBP-g-chitosan

Introduction

Cr(III) and Cr(VI) represent the most common oxidation states of chromium in water. Through food chain transmission and enrichment, the highly toxic hexavalent chromium Cr(VI) species may enter the human body with serious negative impacts to human health (Kimbrough et al. 1999). Cr(VI) is listed as the first category of strictly controlled emission of heavy metal pollutants. Therefore, the proper treatment of Cr(VI) waste represents an important concern in environmental protection and pollution control. Various methods have been developed to remove Cr(VI) form wastewater, including biosorption, chemical or physical adsorption, chemical reduction or bioreduction, electrochemical processes, ion-exchange, and membrane separation techniques (Barrera-Diaz et al. 2012; Jin et al. 2016; Chen et al. 2017; Lyu et al. 2017; Pradhan et al. 2017; Vendruscolo et al. 2017; Xie et al. 2017).

Adsorption represents the most important and effective way for the treatment of Cr(VI). Adsorbents such as MCCS (magnetic ceramsite functionalized with carbon nanospheres), modified activated biochar, modified ramie or chitosan biomass, PEI/CS aerogel beads, nanocarbon materials (magnetic or CNOs), etc., can be used for the efficient removal of hexavalent chromium (Bhatt et al. 2017; Huang et al. 2017; Jiang et al. 2017; Li et al. 2017; Preethi et al. 2017; Sakulthaew et al. 2017; Wu et al. 2017; Zhou et al. 2018). However, conventional adsorption materials exhibit various disadvantages, such as low adsorption capacity, slow adsorption and desorption, long adsorption time, poor selectivity and disability for regeneration and reuse. Therefore, it is of great scientific importance to prepare adsorption materials that are both cost-effective as well as efficient in the removal of Cr(VI) (Azarova et al. 2016; Salehi et al. 2016; Wang et al. 2016; Zhang et al. 2016; Bano et al. 2017; Ma et al. 2017; Wang et al. 2017).

Chitosan, the deacetylated form of chitin, is composed of D-glucosamine units joined by β-(1–4) glucosidic bonds. Due to its low toxicity, biocompatibility and antimicrobial activity, chitosan has been widely applied in the fields of wastewater treatment, membrane separation, antimicrobial agents, biomedical materials, etc.

Chitosan with high content of amine and hydroxyl groups shows good sorption capacity for ordinary transition metal ions including Hg, Co, Ni, Cu, Zn, and Cd, but exhibits a limited sorption capacity properties for anionic oxyspecies (e.g. As and Cr). Thus, the chemical modification of chitosan to achieve the required physical, chemical and mechanical properties, represents a key goal to further enhance the applicability in wastewater treatment strategies. Moreover, chitosan is highly pH sensitive as it can either form a gel or get partly dissolved depending on pH conditions. Suitable modifications of chitosan may result in the production of thin films, fibers, gels, sponges, beads or nanoparticle-based polymeric materials. The preparation of chitosan-based materials generally includes blending, crosslinking, internal hydrogen bonding formation, graft polymerization, etc.

Various chitosan derivatives have been prepared by physical and chemical modification based on active amino groups and hydroxyl groups in the chitosan backbone, which can be used for the treatment of heavy metal ions, such as Hg(II), Cr(VI), and Cu (II) etc. (Ahmad et al. 2015; Li et al. 2015; Ahmad et al. 2016; Lee et al. 2016; Ahmad et al. 2017a, b).

Hyperbranched polymers (HBP) are regarded an important development of polymer science in the twentyfirst century (Hu et al. 2012; Zheng et al. 2015). Owing to a large number of functional groups (amino, hydroxyl, amine, and amide groups), HBP exhibits good chelation properties with divalent metal ions such as Cu(II), Pb(II), Ni(II), Zn(II), Au(II) and Ru(II) (Camarada et al. 2014; López-Cabaña et al. 2015).

The introduction of hyperbranched polymers into the chitosan backbone leads to novel biosorbents for diverse metal ions, such as Hg(II), Pb(II), and Cr(VI) (Ma et al. 2009; Gandhi and Meenakshi 2013; Zarghami et al. 2016). Ma et al. (2009) reported the preparation of a novel PAMAM-g-chitosan biosorbent

material using a divergent method: Michael addition of methyl acrylate to amino groups on the chitosan surface and amidation with ethylenediamine (EDA). Furthermore, the adsorption capability for Pb(II) was studied. Gandhi and Meenakshi (2013) studied the preparation of novel chitosan beads and their Cr(VI) adsorption behaviors. Chitosan was functionalized by amino terminated hyperbranched polyamidoamine (up to 3rd generation) following the same method as described above. Meanwhile, Zarghami et al. prepared different generations of PAMAM-grafted chitosan integrated biosorbents via a step-by-step method using chitosan, methyl acrylate and ethylenediamine as raw materials. Furthermore, PAMAM-grafted chitosan biosorbents were utilized for Pb(II)-removal (Zarghami et al. 2016).

The influence of adsorption conditions (pH value, adsorbent dosage, contact time, initial metal ion concentration) on adsorption properties, adsorption isotherm or kinetics, and adsorption thermodynamics were studied. In general, the active sites in HBP-g-chitosan biosorbent are closely related to free amine and the amide group present in chitosan, structural factors of hyperbranched polymers (end group types, linkers, nuclear unit, and cavity). Furthermore, the distribution of functional groups (amino terminal groups, amide groups) in the hyperbranched polymer skeleton plays a significant role in the adsorption behaviors of the biosorbent. HBP-g-chitosan biosorbents derived from an ethylenediamine core and using a divergent method in heavy metal adsorption, showed obvious disadvantages, including a low grafting rate, poor structure regulation (specific surface area, average pore size, molecular volume), and poor absorption capacities.

Wang et al. (2014, 2015) reported the synthesis of an amino-terminated G0 hyperbranched polymer from diethyl malonate, methyl acrylate, and diethylenetriamine prepared via a two-step synthesis (cf. Fig. 1). The total amine value, secondary amine value and primary amine value of HBP-NH_2 were determined to be 291.59, 210.14, and 81.45 mg/g, respectively. The total amine value was higher than that of the G0 hyperbranched polymer with ethylenediamine core (calculated as 271.1 mg/g), while the structure was more flexible, exhibiting a higher specific surface area and more binding sites for the adsorption of metal ions such as Cr(VI).

In this paper, a tetracarboxylic acid ester was synthesized using diethyl malonate and methyl acrylate. An amino-terminated hyperbranched polymer (HBP-NH_2) was prepared with tetracarboxylic acid ester and diethylenetriamine (DETA). The hyperbranched polymer grafted chitosan (HBP-g-chitosan) was prepared with epichlorohydrin as crosslinking agent for the treatment of Cr(VI). HBP-g-chitosan was characterized by TGA, FT-IR, SEM, XPS, and XRD. The influences of the initial concentration of Cr(VI), HBP-g-chitosan adsorbent concentration, pH value and the competitive anions on the adsorption performance were also discussed. The isotherm of the adsorption process was studied using the Langmuir and Freundlich models. Adsorption kinetics were determined with pseudo-first order and pseudo-two order kinetic models.

Experimental section

Materials

Chitosan (deacetylation degree: 94.13%, molecular weight: 8.41×10^5) obtained from Huantai Shell Products Co. Ltd. (Jinhu County, Zhejiang, China) was dried at 85 °C in a vacuum oven for 8 h to remove any residual water content (Xu et al. 2016).

Diethyl malonate, methanol, tetra-n-butylammonium bromide, methyl acrylate (MA), epichlorohydrin (ECH), and diethylenetriamine (DETA) were purchased from Sinopharm Chemical Reagent Co., Ltd. Potassium dichromate, potassium carbonate, and

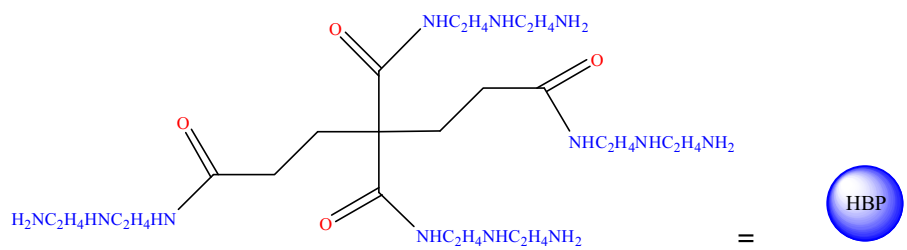

Fig. 1 Structure of G0 HBP-NH_2

sodium hydroxide were purchased from Shanghai Aladdin Industrial Chemical Co., Ltd. All reagents were of Analytical Reagent grade.

Preparation of HBP-g-chitosan

HBP-g-chitosan was prepared via a two steps synthesis, (1) preparation of HBP-NH_2 with diethyl malonate, MA, and DETA according to the literature (Wang et al. 2014, 2015), and (2) preparation of HBP-g-chitosan from HBP-NH_2 and chitosan with ECH as crosslinking agent. The corresponding synthesis procedure is shown in Fig. 2.

First, Michael addition of a tetracarboxylic ester (cf. Fig. 2a) was carried out with petroleum ether as solvent, tetra-n-butylammonium bromide as phase transfer catalyst, and potassium carbonate as base. Then HBP-NH_2, a yellow viscous liquid, was synthesized from tetracarboxylic ester and DETA with methanol as solvent (cf. Fig. 1).

In a 500 mL four-neck round-bottomed glass flask, chitosan (1.5 g) was dissolved in 2% aqueous acetic acid (50 mL) and HBP-NH_2 (6 g) was added thereafter. The mixture was stirred for 1 h at room temperature. Then, the temperature was raised to 40 °C and ECH (6 g) was slowly added into the flask. The mixture was stirred for 5 h at 70 °C and then cooled and filtered. HBP-g-chitosan (Fig. 2b) was obtained by washing the solid residue with deionized water, and drying at 80 °C in a vacuum oven for 12 h.

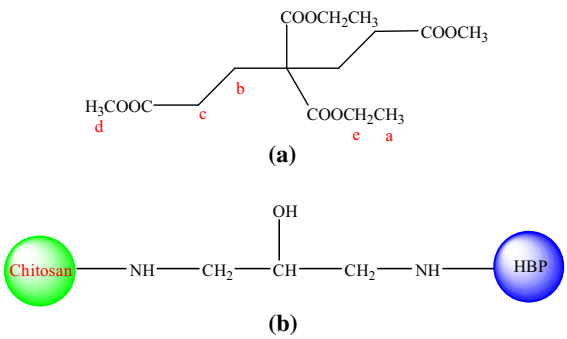

Fig. 2 Schematic structure: **a** tetracarboxylic ester, **b** HBP-g-chitosan

Material characterization

The chemical structure of tetracarboxylic ester was characterized by ^{1}H-NMR. ^{1}H-NMR spectra were recorded on an AVANCE AV-500 (Bruker Co. Ltd., Germany) operating at 500 MHz. Chemical shifts are provided in ppm units relative to tetramethylsilane (TMS). The splitting patterns were designated as follows: s (singlet), d (doublet), t (triplet), q (quartet), and m (multiplet).

FT-IR spectra of chitosan and HBP-g-chitosan were recorded on a Nicolet 5700 FT-IR spectrometer (Thermo Electron Corporation, Madison, WI, USA). For each spectrum, 64 scans were recorded over a range of 4000–500 cm^{-1} at 22 °C at a resolution of 4 cm^{-1}. A background spectrum was recorded on air and subtracted from the sample spectrum.

A Mettler Toledo TGA Q50 machine (Mettler-Toledo Ltd., Port Melbourne, Australia) was used with 40 µL aluminium crucibles for thermogravimetric analysis (TGA) under nitrogen. A sample mass of about 5 mg was used for each run. The samples were heated from 40 to 500 °C and measured in a dynamic heating regime, using a constant heating ramp of 10 K/min.

XRD patterns were collected on a Smart Lab 2kw XRD diffractometer with Cu Kα radiation (λ = 0.154 nm) over the range of 5°–60° (2θ) and at a scan speed of 2° (2θ) per minute.

SEM photomicrographs were recorded on a TM3000 scanning electron microscope (FEI Instrument Co., Ltd., USA) at an accelerating voltage of 20 kV. The free surfaces of the regenerated chitosan were coated with thin layers of gold before observation.

A Kratos AXIS Ultra DLD Multifunctional X-ray Photoelectron Spectrometer (Manchester, UK) using monochromatic Al Kα X-rays (1480 eV) was used to study the adsorption mechanism of the chitosan-based adsorbent. C, O, N, Cl and Cr for each sample were scanned (binding energy, 0.00–1100.00 eV; scanning speed, 0.65 eV/150 mS; two times), and XPS peak software (version 4.1) was used to fit the spectra peaks to identify the different oxidation states of each element. The binding energy scale for the final calibration was corrected by the C1s peak corresponding to 284.8 eV.

Cr(VI) adsorption experiments

A series of batch adsorption experiments were carried out by adding aqueous solutions of Cr(VI) ions (50 mL) and a quantitative HBP-g-chitosan to the flasks with different contact time. The pH of the above solution was adjusted by adding HCl or NaOH solutions (0.1 M).

The influences of the initial concentration of Cr(VI), dosage of adsorbent, pH and the coexisting anions on the adsorption performance were studied. The effect of initial Cr(VI) concentration was conducted by placing different concentrations of an aqueous solution of Cr(VI) (from 20 to 220 mg/L with 40 mg/L interval) and 50 mg of HBP-g-chitosan at pH = 5.0. The effect of the quality of HBP-g-chitosan was studied by adding an aqueous solution of Cr(VI) (100 mg L^{-1}) and different quantities of HBP-g-chitosan (from 10 to 60 mg) at pH = 5.0. Meanwhile, the effect of pH was measured from 2.0 to 6.0 and the effect of competitive anions was studied by adding Ac^-, HSO_3^-, Cl^- and SO_4^- (10 mg/L) to the solution. The bottles were sealed with rubber stoppers and equilibrated on a shaker at 200 rpm. The corresponding Cr(VI) concentration was determined using a UV–visible spectrophotometer (Cary60, Agilent) at 540 nm, according to the 1,5-diphenyl-carbazide method. In order to ensure the reproducibility of all results, experiments were conducted in triplicate and the mean value of these independent tests was used for analysis.

The adsorption capacity and removal rate were calculated by the following equation:

$$Q_t = (\rho_0 - \rho_t) \cdot V/m \quad (1)$$

$$r = \frac{\rho_0 - \rho_t}{\rho_0} \times 100\% \quad (2)$$

where Q_t is the unit adsorption capacity (mg/g), r is the removal rate of Cr(VI), ρ_0 and ρ_t are the initial Cr(VI) concentration (mg/L) and Cr(VI) concentration at time t (mg/L), respectively. V is the volume of Cr(VI) solution (L), and m is the weight of HBP-g-chitosan (g).

Adsorption isotherms

Langmuir and Freundlich adsorption isotherm models were used to study the thermodynamics of the Cr(VI) adsorption process. The adsorption process was conducted using 50 mg HBP-g-chitosan with various Cr(VI) concentrations (20–220 mg/L) and a contact time of 10 h at pH = 5.0 and 30 °C.

Adsorption kinetics

Pseudo-first order and pseudo-second order kinetic models were used to study the kinetics of the adsorption process of Cr(VI). The adsorption process was carried out using 50 mg of adsorbent with a Cr(VI) concentration of 100 mg/L at pH = 5.0 and 30 °C. The Cr(VI) concentrations in solutions were determined at various time intervals (30 min interval from 0 to 2 h, and 120 min interval from 2 to 10 h).

Desorption and regeneration of HBP-g-chitosan adsorbent

For desorption and regeneration, HBP-g-chitosan adsorbent was used for successive adsorption–desorption cycle experiments (Chen et al. 2013; Debnath et al. 2014). For adsorption experiments, 50 mL of 100 mg/L Cr(VI) solution was adsorbed with 1.0 g/L HBP-g-chitosan at pH = 5.0. After 120 min of adsorption, the HBP-g-chitosan adsorbent was carefully separated from the solution and washed thoroughly. Thereafter, desorption experiments were performed with 50 mL of different concentration sodium hydroxide (NaOH) solutions (0.05, 0.1, 0.2, and 0.4 M, respectively) brought in contact with the HBP-g-chitosan adsorbent. Desorption experiments were maintained for 120 min. At the end of each adsorption–desorption cycle, the HBP-g-chitosan adsorbent was washed with deionized water to remove any excess NaOH from the adsorbent surface. The desorbed Cr(VI) was determined as mentioned in section "Cr(VI) adsorption experiments". The reusability of HBP-g-chitosan for Cr(VI) adsorption was evaluated by conducting five consecutive adsorption–desorption cycles.

Results and discussion

Characterization of materials

^{1}H NMR spectroscopic data

The ^{1}H-NMR spectrum of the tetracarboxylic ester is shown in Fig. S1 and all corresponding parameters are listed in Table S1. Locations of hydrogen in tetracarboxylic ester are shown in Table S1 (a, b, c, d, and e). ^{1}H-NMR (DMSO-d_6): 1.16 ppm (t, 3H), 2.05 ppm (t, 2H), 2.24 ppm (t, 2H), 3.59 ppm (s, 3H), and 4.11 ppm (d, 2H).

FT-IR spectra

FTIR spectra of chitosan and HBP-g-chitosan are shown in Fig. 3. The peaks at 1735 cm^{-1} (C=O stretching vibration of the ester bond) and 1244 cm^{-1} (C–O–C stretching vibration of the ester bond) could not be found in Fig. 3a. However, the peak at 1544 cm^{-1} could be assigned to N–H bending vibration of the primary amine, indicating that HBP-NH_2 was successfully grafted to the chitosan backbone.

The solubility of chitosan and HBP-g-chitosan in different solvents is shown in Table S2. As shown here, chitosan was soluble in 2% acetic acid and trifluoroacetic acid + DMF (3:1). HBP-g-chitosan was soluble in trifluoroacetic acid + DMF (3:1) but insoluble in 2% acetic acid. Further solubility tests confirmed the successful grafting of HBP-NH_2 to chitosan.

Product photos of chitosan and HBP-g-chitosan are shown in Fig. S2. Chitosan was obtained as a pale yellow powder (Fig. S2a), while HBP-g-chitosan was obtained as solid particles with dark yellow color (Fig. S2b).

TGA characterization

TGA and DTG of chitosan and HBP-g-chitosan are shown in Figs. 4 and S3. Two weight loss steps could be observed in chitosan and HBP-g-chitosan. Minor weight loss of chitosan and HBP-g-chitosan occurred at around 100 °C, corresponding to 2.3 and 0.4% loss, respectively. The latter finding may be attributed to the loss of adsorbed and bound water. Significant weight loss of chitosan could be observed at 286 °C and stabilized at 330 °C. This weight loss could be

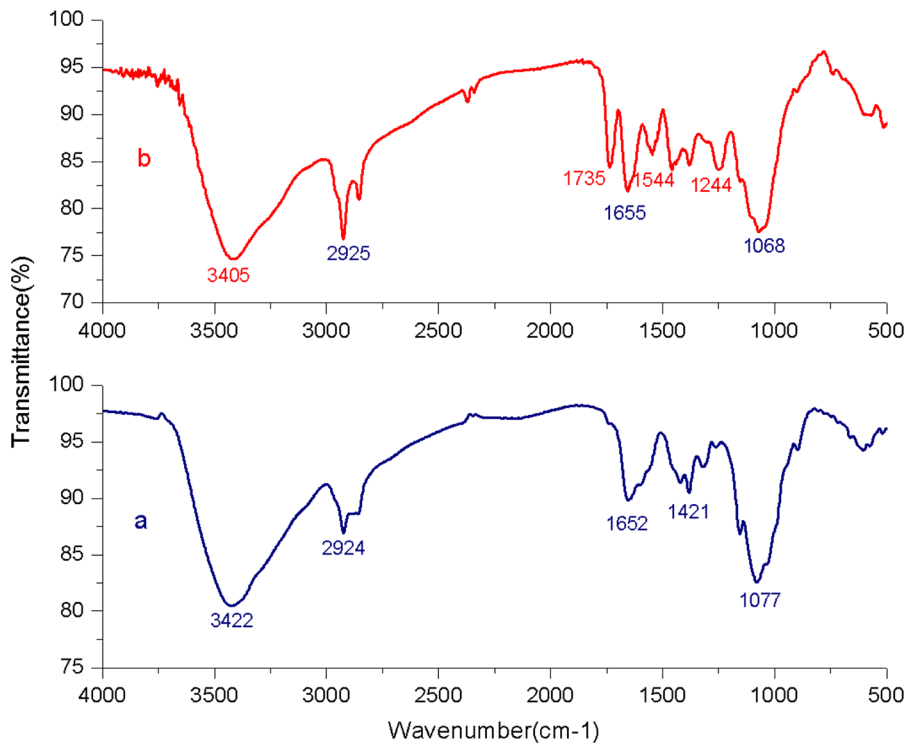

Fig. 3 FTIR spectra: **a** chitosan, **b** HBP-g-chitosan

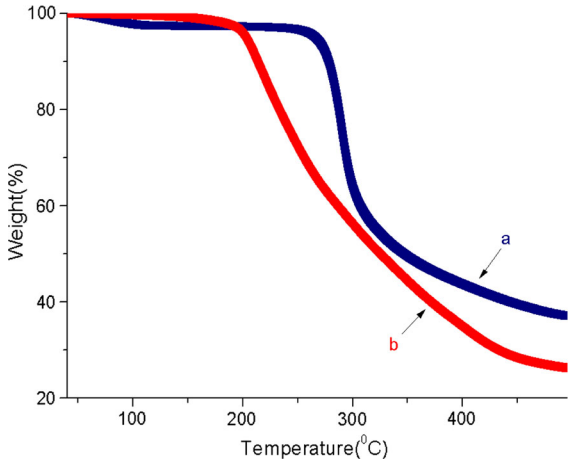

Fig. 4 TGA of samples: **a** chitosan, **b** HBP-g-chitosan

attributed to the melting, deacetylation, and decomposition of chitosan. Significant weight loss of HBP-g-chitosan was observed at 228 °C, a lower temperature than was observed for chitosan. The reason for this may be due to the graft of HBP-NH_2 to chitosan since more flexible hyperbranched polymer units were introduced into the chitosan backbone. In this context, He et al. (He et al. 2016) found that the decomposition temperature generally decreases when a hyperbranched polyamidoamine polymer is introduced into the chitosan backbone.

XRD characterization

XRD characterization data of chitosan, HBP-g-chitosan adsorbent, and Cr(VI) loaded to HBP-g-chitosan (abbreviated as CrLHCh) is shown in Fig. 5. Two main diffraction peaks at 2θ = 10.5° and 19.8° (shown in Fig. 5a), assigned to (0 2 0) and (1 0 0) crystallographic planes, represent typical crystalline domains of native chitosan (Xu et al. 2016). HBP-g-chitosan and CrLHCh showed two main diffraction peaks at 2θ = 10.0° and 22.5° (shown in Fig. 5b, c). The crystallization degree of HBP-g-chitosan decreased sharply, most likely due to the graft of HBP-NH_2 on chitosan.

SEM of chitosan, HBP-g-chitosan, and CrLHCh

The SEM surface morphology (magnification 2000×) of chitosan, HBP-g-chitosan, and CrLHCh is shown in Fig. 6. Compared to chitosan (cf. Fig. 6a), the surface morphology of HBP-g-chitosan (cf. Fig. 6b) displayed

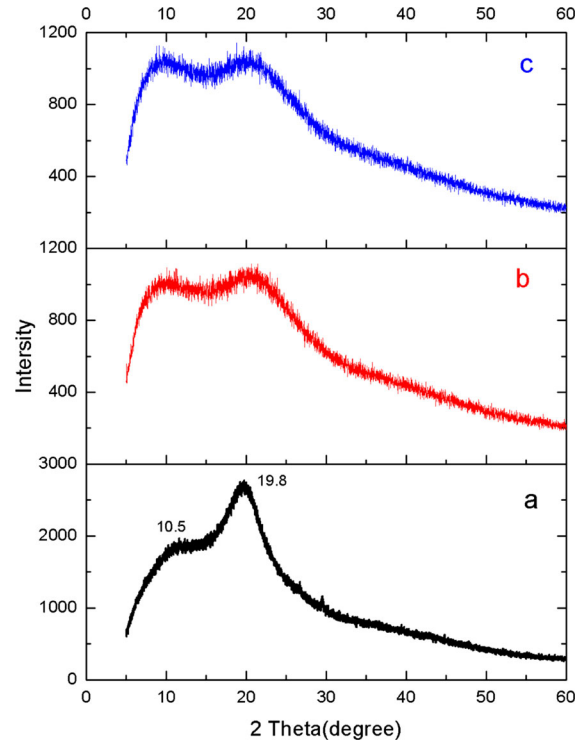

Fig. 5 XRD characterization: **a** chitosan, **b** HBP-g-chitosan, and **c** CrLHCh

a porous morphology at the same magnification, suggesting that the adsorbent might exhibit a higher surface area and higher adsorption properties. The surface morphology of CrLHCh (cf. Fig. 6c) demonstrated the presence of a large number of holes leading to a higher Cr(VI) adsorption.

XPS of chitosan, HBP-g-chitosan, and CrLHCh

Figure 7 and Table 1 summarize the XPS data of chitosan, HBP-g-chitosan, and CrLHCh, including binding energies and peak area.

The Cr 2p3/2 peak at 576.47 and 2p1/2 peak at 586.59 were observed as shown in Fig. S4. BEs for Cr 2p3/2 could be assigned to Cr(III) at 576.47 eV, while Cr(VI) was characterized at higher binding energies of 586.59 eV. It is possible to assume that Cr(VI) was partially reduced to Cr(III) [about 66.9% calculated from the peak area in Table 1]. In this context, Li et al. (Li et al. 2015) found the same Cr(VI) reduction to Cr(III) using electrospinning nanosized chitosan fibers.

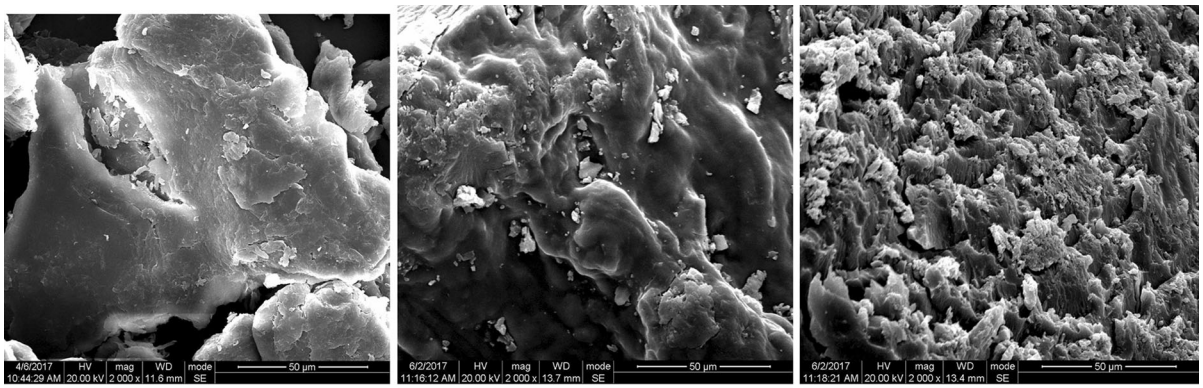

Fig. 6 SEM surface morphology (magnification 2000×): **a** chitosan, **b** HBP-g-chitosan, and **c** CrLHCh

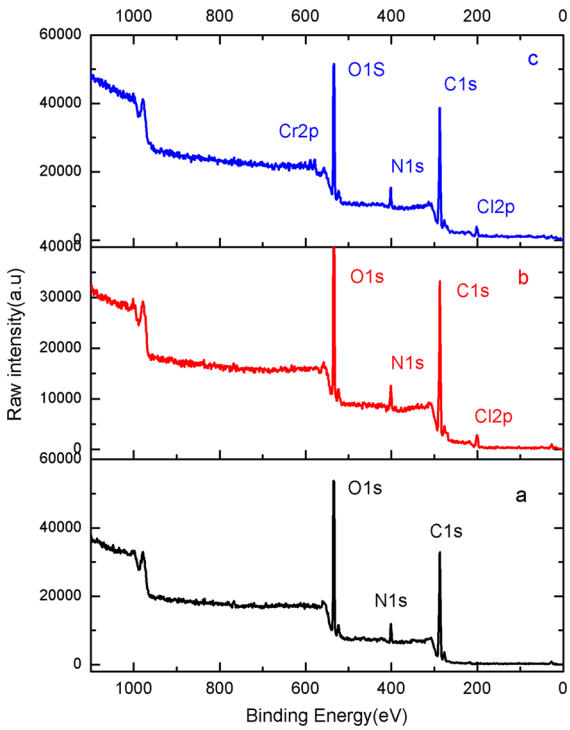

Fig. 7 XPS spectra: **a** chitosan, **b** HBP-g-chitosan, and **c** CrLHCh

For the N1 s spectra (as shown in Fig. S5), two peaks of chitosan could be observed at BE 399.01 and 400.21 eV. Both could be attributed to $–NH_2$ or NH groups and a protonated $–NH_2$ group ($–NH_3^+$) (Fig. S5a). As for the N1s spectra of HBP-g-chitosan (Fig. S5b), the N1s binding energy and peak area changed significantly. A higher binding energy of 401.34 eV was observed, suggesting the presence of a new bond involving the atom N. The peak area of N1 s increased sharply from 5368.03 to 9670.67 due to the graft between HBP-NH_2 and the chitosan backbone. For the N1s spectra of CrLHCh (cf. Fig. S5c), three peaks at BE 398.70, 400.10, and 401.59 eV could be observed, indicating the interaction between chromium and the amino group. However, a peak of low intensity was observed at a BE of 401.59 eV which could be attributed to the formation of a chromium–NH_2 complex. The appearance of the N peak at higher binding energy is indicative of reduction in the electron cloud density of the nitrogen atom, probably due to the utilization of its lone pair in the formation of a new bond between N and Cr(VI) (Vieira et al. 2011; Shen et al. 2013; Bhatt et al. 2015; Lee et al. 2016).

As shown in Fig. S6, two O1s peaks of chitosan and HBP-g-chitosan at BE 531.5 and 532.6 eV could be observed, which could be attributed to the presence of –OH and C–O groups (cf. Figs. S6a and S6b). The O1s spectrum of Cr(VI) adsorption was deconvoluted into two peaks at 531.29 and 533.21 eV (cf. Fig. S6c). The binding energy at 533.21 eV was attributed to the formation of $Cr(OH)_3$ (Vieira et al. 2011; Shen et al. 2013; Bhatt et al. 2015). The binding energy increased after chromium adsorption, indicating that the hydroxyl group was involved in the adsorption.

For Cl2p spectra of HBP-g-chitosan and CrLHCh (shown in Fig. S7), the existence of Cl2p spectra confirmed the successful graft between HBP-NH_2 and the chitosan backbone. As shown in Fig. S7b, there were two Cl2p peaks of HBP-g-chitosan at BE of 197.24 and 199.50 eV, which could be attributed to the formation of an ammonium salt. There were two

Table 1 XPS information of Chitosan, HBP-g-chitosan, and CrLHCh

Materials	Atom	Binding energy (eV)	FWHM	Peak area
Chitosan	O	531.54	1.05	11,527.92
		532.70	1.32	31,376.79
	N	399.01	1.58	4091.29
		400.21	1.32	1276.74
HBP-g-chitosan	O	531.51	1.49	18,164.98
		532.57	1.62	32,229.19
	N	399.12	1.89	7265.96
		401.34	1.78	2404.71
	Cl	197.24	1.42	1780.63
		199.50	1.78	2259.69
CrLHCh	O	531.29	1.68	26,273.18
		533.21	1.34	16,168.4
	N	398.70	1.45	3403.18
		400.10	1.52	3212.31
		401.59	0.95	584.09
	Cl	197.73	1.57	1411.98
		199.97	1.6	1078.57
	Cr	576.47	2.65	1850.92
		586.60	2.51	915.67

Cl2p peaks of CrLHCh at BE of 197.73 and 199.97 eV (cf. Fig. S7c), corresponding to the formation of $CrCl_3$.

Cr(VI) adsorption studies

Effect of initial concentration of Cr(VI)

Figure 8 shows the adsorption capacity and removal rate of Cr(VI) at different initial concentrations (20–220 mg/L in 40 mg/L intervals) at 30 °C (adsorbent concentration: 1 g/L, at pH = 5.0). Notably, the higher the initial concentration of Cr(VI), the greater the adsorption capacity of Cr(VI) at the same adsorption time. The adsorption capacity of Cr(VI) increased greatly within the first 120 min, then the adsorption rate of Cr(VI) increased gradually and was stable after 360 min. The maximum adsorption capacity was 18.75, 48.07, 83.58, 110.12, 125.98, and 160.21 mg/L, respectively, for different initial Cr(VI) concentrations. The removal rate was 93.8, 80.1, 83.58, 78.66, 70.0, and 72.8%, respectively. The Cr(VI) adsorption capacity of various chitosan-based adsorbents can be found summarized in Table 2 (Sankararamakrishnan and Sanghi 2006; Kousalya et al. 2010; Chauhan et al. 2012; Shen et al. 2013; Thinh et al. 2013; Zhang et al. 2013; Bhatt et al. 2015). The adsorption capacity and removal rate of HBP-g-chitosan was much higher than chitosan crosslinked with DTPA adsorbent (Bhatt et al. 2015), while lower than Zr-chitosan (Zhang et al. 2013).

Effect of HBP-g-chitosan dosage

Figure 9 shows the adsorption capacity of Cr(VI) with different dosage of HBP-g-chitosan (0.2, 0.6, and 1.0 g/L) at pH = 5.0 (initial concentration: 100 mg/L at 30 °C). As shown in Fig. 9, the adsorption capacity of Cr(VI) increased sharply within the first 120 min, then increased gradually for different dosages of HBP-g-chitosan. In addition, the adsorption capacity of Cr(VI) decreased at same contact time when the quantity of HBP-g-chitosan was increased. The results indicate that the active adsorption site increased upon increasing the adsorbent dosage. However, when the adsorbent dosage increased to a certain extent, the adsorption sites were not completely occupied by Cr(VI).

pH effect

The effect of pH on the adsorption capacity of Cr(VI) was studied from pH = 2.0–6.0 (adsorption condition:

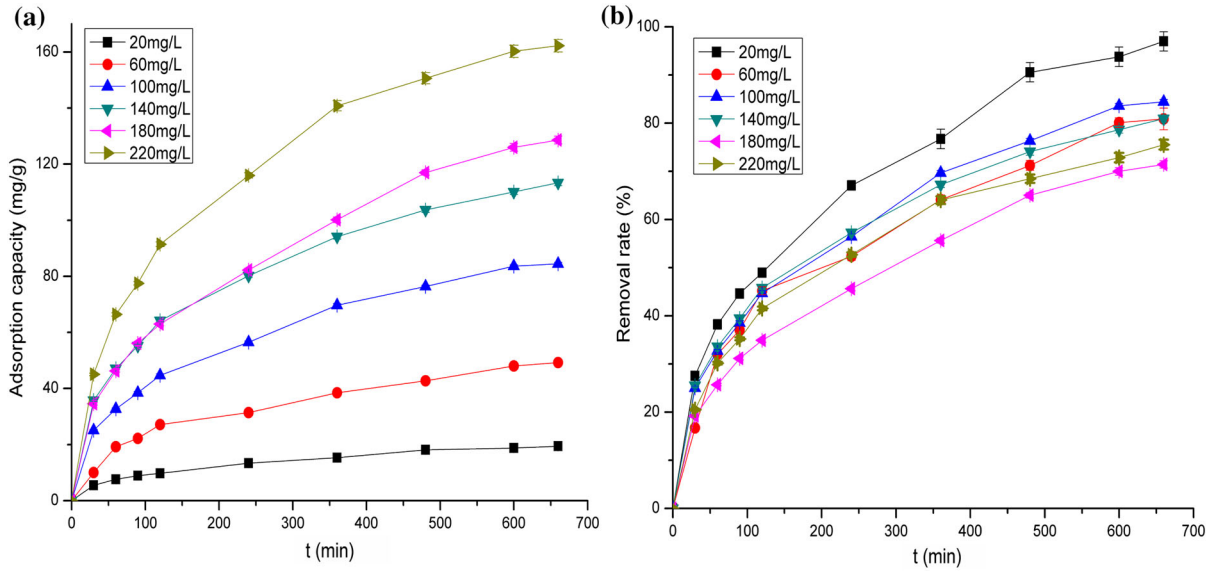

Fig. 8 Adsorption capacity (**a**) and removal rate (**b**) of Cr(VI) at different initial concentrations

Table 2 Summary for Cr(VI) adsorption capacity of various chitosan-based adsorbents

Adsorbents	Form	Process parameters	Qmax	Removal rate (%)	Reference
Magnetic chitosan	Nanoparticle	pH = 3.0; I.C. = 180 mg/L; D.A. = 2 g/L	55.8 mg/g	31	Jiang et al. (2017), Xie et al. (2017)
Chitosan bead grafted with ethylenediamine	Bead	pH = 5.0; I.C. = 10 mg/L; D.A. = 2 g/L	9.3 mg/g	93	Xu et al. (2016)
Xanthated Chitosan	Bead	pH = 3.0; I.C. = 100 mg/L; D.A. = 5 g/L	71 mg/L	71	Zarghami et al. (2016)
Thiocarbamoyl chitosan	Flake	pH = 2.0; I.C. = 1000 mg/L; D.A. = 1 g/L	434.8	43.5	Zhang et al. (2016)
Electrospun chitosan nanofibers	Mat	pH = 4.5; I.C. = 100 mg/L; D.A. = 1 g/L	68.3	68.3	López-Cabaña et al. (2015)
Chitosan-Fe(III) complex	Powder	pH = 4.8; I.C. = 500 mg/L; D.A. = 1 g/L	173.1	34.6	Wen et al. (2011)
Chitosan crosslinked with DTPA	Powder	pH = 3.0; I.C. = 500 mg/L; D.A. = 2 g/L	192.3	38.5	Wu et al. (2017)
Zr-chitosan	Powder	pH = 5.0; I.C. = 200 mg/L; D.A. = 0.08 g/L	175.0	87.5	Zhang et al. (2013)
3ACBZr	Bead	pH = 4.0; I.C. = 200 mg/L; D.A. = 1 g/L	185.0	92.5	Thinh et al. (2013)
G0 HBP-g-chitosan	Powder	pH = 3.0; I.C. = 220 mg/L; D.A. = 1 g/L	194.6	88.5	This work

I.C. initial concentration, *D.A.* dosage of absorbent

initial concentration = 100 mg/L, 50 mg adsorbent, contact time 300 min at 30 °C).

As shown in Fig. 10, the Cr(VI) uptake increased slightly from pH = 2.0–3.0, then decreased sharply from pH = 3.0–6.0. The maximum adsorption

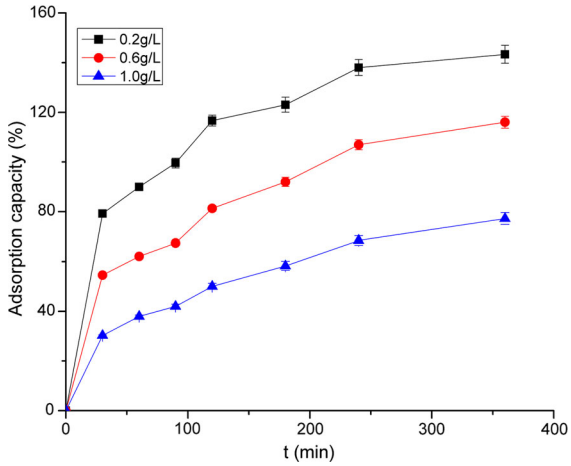

Fig. 9 Adsorption capacity of Cr(VI) at different dosage of HBP-g-chitosan

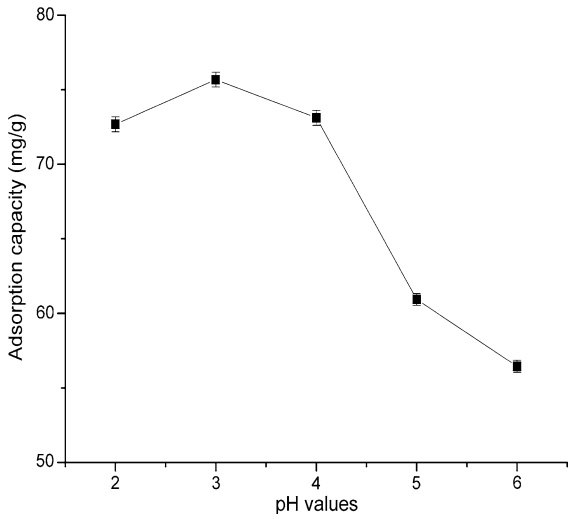

Fig. 10 Effect of pH on adsorption capacity of Cr(VI)

capacity of Cr(VI) on HBP-g-chitosan adsorbent occurred at pH = 3.0.

Generally appreciated is the fact that the pH of the Cr(VI) solution affects the adsorption performance since the pH affects the speciation of ionic chromium species ($Cr_2O_7^{2-}$, $HCrO_4^-$, CrO_4^{2-}, or $HCr_2O_7^-$), the degree of chromium ionization, and the surface charge of HBP-g-chitosan adsorbent (Kousalya et al. 2010; Li et al. 2015).

When pHs are below 5.0, the amino groups can easily be protonated to NH_3^+ and Cr(VI) appears mainly as $HCrO_4^-$, CrO_4^{2-}. A strong electrostatic attraction exists between the oxyanions of Cr(VI) and the positively charged surface of HBP-g-chitosan adsorbent. The latter demonstrates the main adsorption mechanism of Cr(VI) ions onto HBP-g-chitosan adsorbent. Upon increasing the pH, the degree of protonation of the NH_2 group in the adsorbent reduces gradually, resulting in a sharp decrease of Cr(VI) adsorption capacity. The slight increase in Cr(VI) adsorption from pH = 2.0 to pH = 3.0 can be explained by the fact that Cr(VI) exists as H_2CrO_4 (neutral state) at pH $\leq$ 3.0 and cannot interact with $-NH_3^+$, resulting in a decrease in Cr(VI) adsorption (Zimmermann et al. 2010; Wen et al. 2011).

Effect of competitive anions

The presence of anions may decrease the adsorption capacity of Cr(VI) due to competing effects to interact with active sites on the surface of HBP-g-chitosan. To investigate such an effect, different anions (Cl^-, HSO_3^-, SO_4^{2-}, and Ac^- in the form of NaCl, $NaHSO_3$, Na_2SO_4, and NaAc) were added to Cr(VI) solutions. The concentration of the anions was 10 mg/L. The corresponding effect of competitive anions on adsorption capacity of Cr(VI) is shown in Fig. 11.

The adsorption capacity of Cr(VI) reduced upon addition of competitive anions. The adsorption capacity decreased from 69.69 mg/g (absence of anions) to 66.92 mg/g (Cl^-), 57.73 mg/g (HSO_3^-), 56.87 mg/g (SO_4^{2-}), and 50.25 mg/g (Ac^-). The decreasing trend of the adsorption capacity of Cr(VI) in the presence of

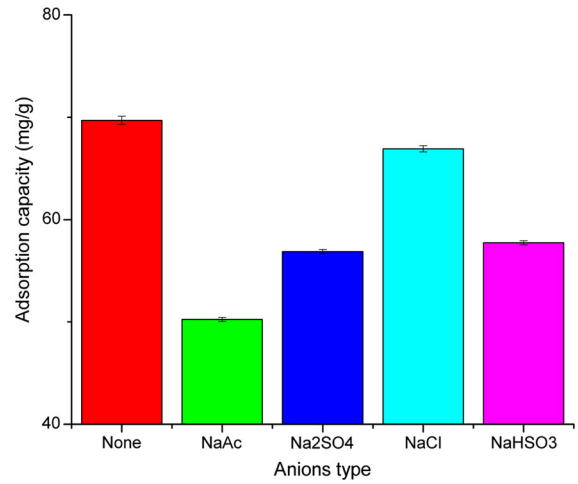

Fig. 11 Effect of competitive anions on adsorption capacity of Cr(VI)

competitive anions was observed in the order of: Cl^- < HSO_3^- < SO_4^{2-} < Ac^-.

The adsorption capacity of Cr(VI) decreased only 3.97% when Cl^- was present, indicating the high affinity of HBP-g-chitosan to bind to Cr(VI) ions existing as $HCrO_4^-$ at pH = 5.0. However, Cr(VI) adsorption was greatly affected with the presence of HSO_3^-, SO_4^{2-}, and Ac^-. This finding indicates a strong competition between Cr(VI) and HSO_3^-, SO_4^{2-}, and Ac^-. As reported previously (Li et al. 2015; Gandhi and Meenakshi 2013), HSO_3^-, SO_4^{2-}, and Ac^- can crosslink with protonated amino groups in chitosan, thus decreasing the number of the binding sites of chitosan for the adsorption of Cr(VI). The HSO_3^- anion is likely to dissociate to form a proton that may affect the speciation of the ionic chromium species (increase of $HCrO_4^-$, CrO_4^{2-}).

Adsorption isotherm and kinetics study

Adsorption isotherm study

The Freundlich and Langmuir models were adopted for the determination of Cr(VI) adsorption capacity of HBP-g-chitosan at different initial concentrations (20–220 mg/L at 40 mg/L interval) at 30 °C (adsorbent concentration: 1 g/L at pH = 5.0).

The Langmuir and Freundlich adsorption isotherm models are shown in Fig. S8, and the values of relevant parameters are listed in Table 3.

Freundlich isotherm constants for HBP-g-chitosan were calculated from the linear plot of ln Qe versus lnρe (Kousalya et al. 2010; Zarghami et al. 2016). The conditions were found to be favorable for adsorption because the value n was greater than 1. The K_F value was 22.31, indicating the applicability of the Freundlich isotherm.

The Langmuir isotherm constants Q_{max} and K_L for HBP-g-chitosan determined from the respective slope and intercept of the linear plot of ρe/Qe versus ρe (Kousalya et al. 2010; Zarghami et al. 2016). These values are presented in Table 3. The Qmax for HBP-g-chitosan was 194.55 mg/g, which was higher than Zr-chitosan and 3ACBZr adsorbents (175.0 mg/m and 185.0 mg/g, respectively) at the same Cr(VI) initial concentration (200 mg/L, shown in Table 2) (Gandhi and Meenakshi 2013; Zhang et al. 2013). The K_L values between 0 and 1 indicated that the conditions were favorable for adsorption. The higher R^2 values of the Freundlich over the Langmuir isotherm indicated the higher applicability of the Freundlich isotherm compared to the Langmuir isotherm.

Table 3 Parameters for Langmuir and Freundlich

Model	Relevant parameters	R^2
Langmuir	Q_{max} = 194.55, K_L = 0.0514	0.7359
Freundlich	n = 2.174, K_F = 22.31	0.9205

Equilibration time, 600 min

Adsorption kinetics study

Two kinetic models such as pseudo-first order and pseudo-second order were applied to determine the kinetic rate uptake of Cr(VI) onto HBP-g-chitosan adsorbent (Kousalya et al. 2010; Zarghami et al. 2016). The adsorption capacity as a function of contact time at an initial concentration of 100 mg/g and pH = 5.0 (adsorbent concentration: 1.0 g/L) is shown in Fig. 9. As shown here, by increasing time, the adsorption capacity increased and at a certain time (120 min) reached a maximum adsorption capacity and became almost constant thereafter.

The kinetic parameters for the pseudo-first and pseudo-second models were determined from the linear plots of ln (Qe-Qt) versus t and (t/Qt) versus t from the experimental data described in section "Effect of HBP-g-chitosan dosage". The values of K_1, K_2, R^2, Qe(exp), and Qe(cal) are shown in Table 4.

As shown in Table 4, Figs. S9a and b, the calculated Qe (Qe(cal) = 91.158 mg/g) of the pseudo-second order model was more favorable to the value of the pseudo-first order model (Qe(cal) = 69.839 mg/g). This latter finding indicated that the pseudo-second order model was more valid to describe the kinetics of the undergoing Cr(VI) adsorption process. The R^2 value obtained indicates a higher suitability for the pseudo-first order model.

The more reliable adsorption kinetics of the pseudo-second order equation implies that the rate limiting step was chemisorption, involved the formation of covalent bonds through the sharing or exchange of electrons between Cr(VI) and HBP-g-chitosan.

Table 4 Parameters for kinetic models

ρ_0/mg L^{-1}	Qe(exp)	Pseudo-first order			Pseudo-second order		
		K_1	R^2	Qe (cal)	K_2	R^2	Qe (cal)
100	84.438	4.36×10^{-3}	0.9916	69.839	9.77×10^{-5}	0.9795	91.158

Desorption and regeneration of HBP-g-chitosan adsorbent

Reusability evaluation of the adsorbent is a primary condition to develop a practical and economical adsorbent. Different concentrations of NaOH solutions (0.05–0.4 M) were used to desorb Cr(VI) from the HBP-g-chitosan adsorbent (Chen et al. 2013; Debnath et al. 2014; Zhang et al. 2016).

Desorption of Cr(VI) from HBP-g-chitosan adsorbent using different concentrations of NaOH solutions (0.05–0.4 M), and regeneration of HBP-g-chitosan adsorbent using 0.2 M NaOH are shown in Fig. 12.

As shown in Fig. 12a, 0.2 M NaOH was found to be the optimum concentration for effective Cr(VI) desorption.

Cr(VI) adsorption percentage (compared to the initial adsorption capacity) with regenerated HBP-g-chitosan adsorbent for five consecutive adsorption–desorption cycles is shown in Fig. 12b.

As shown here, the Cr(VI) adsorption capacity remained constant for three cycles of adsorption–desorption. The Cr(VI) adsorption capacity was about 96% of the initial adsorption capacity. For the fourth and fifth cycle of regeneration, the adsorption capacity decreased to 89.3 and 85.6% of the initial adsorption capacity. This result indicates that the HBP-g-chitosan adsorbent may be considered to be an efficient recyclable adsorbent for Cr(VI) removal from wastewater.

Adsorption mechanism

The adsorption of Cr(VI) onto HBP-g-chitosan adsorbent took place in three consecutive steps:

1. Binding of anionic Cr(VI) (mainly $Cr_2O_7^{2-}$, $HCrO_4^-$) to the protonated, positively charged amino groups on the HBP-g-chitosan surface promoted by electrostatic attraction;

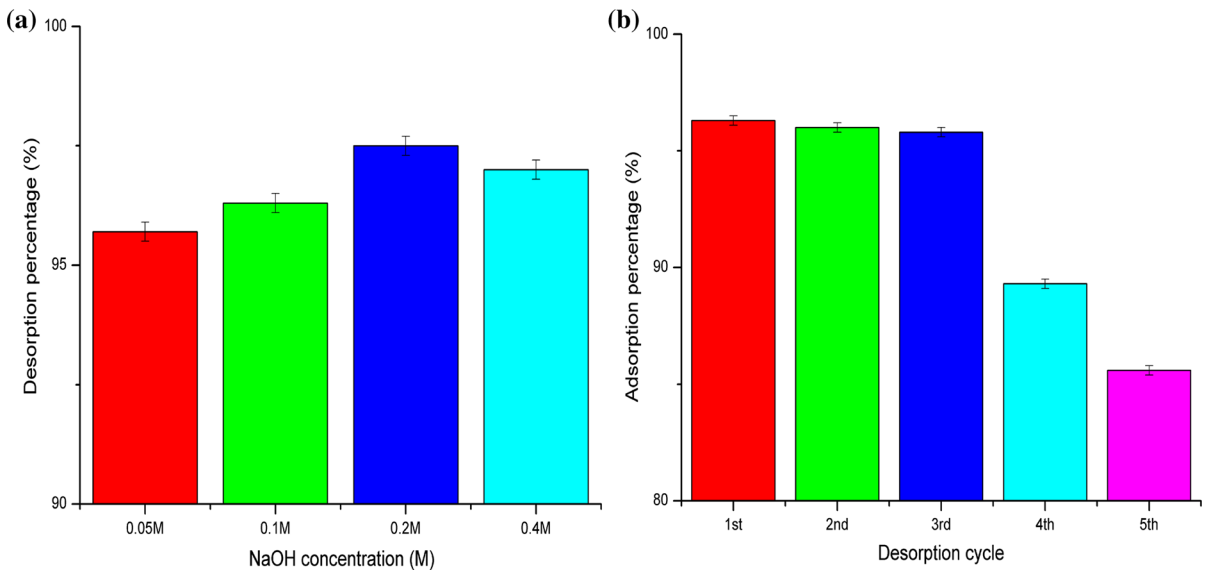

Fig. 12 **a** Desorption of Cr(VI) from adsorbent using different NaOH concentrations, and **b** regeneration of HBP-g-Chitosan adsorbent using 0.2 M NaOH

2. Reduction of Cr(VI) to Cr(III) by adjacent electron-donor groups;
3. Formation of Cr(III) complex with functional groups (amino, carboxyl, hydroxyl, and amide) in adsorbent. The amino group played an important role in the reduction of Cr(VI)–Cr(III) (Kousalya et al. 2010; Bhatt et al. 2015; Zarghami et al. 2016).

Conclusions

In this paper, tetracarboxylic acid ester was synthesized by reaction of diethyl malonate with methyl acrylate and the resulting material was characterized by ^{1}HNMR. An amino terminated hyperbranched polymer (HBP-NH_2) was synthesized by reaction of a tetracarboxylic acid ester with diethylenetriamine (DETA). HBP-g-chitosan, a novel biosorbent, was prepared for the treatment of Cr(VI). HBP-g-chitosan was characterized by TGA, FTIR, SEM, XPS, and XRD. The influence of the initial concentration of Cr(VI), HBP-g-chitosan concentration, pH value and the competitive anions on the adsorption performance were discussed. The results showed that the adsorption capacity of Cr(VI) gradually increased, whereas the removal rate gradually decreased upon addition of the initial concentration of Cr(VI) at the same contact time. Furthermore, the adsorption capacity of Cr(VI) gradually decreased upon increasing the HBP-g-chitosan concentration at the same contact time. It was determined that the pH value played an important role in the HBP-g-chitosan adsorption process as the pH affected the speciation of ionic chromium species, the degree of chromium ionization, and the surface charge of the HBP-g-chitosan adsorbent. The removal rate of Cr(VI) was shown to reduce after the addition of competitive anions and this decreasing trend for the removal rate of Cr(VI) in the presence of competitive anions was observed in the following order: $Cl^- < HSO_3^- < SO_4^{2-} < Ac^-$.

Langmuir and Freundlich models were applied to generate a Cr(VI) adsorption isotherm. The results indicated that the Freundlich model was more suitable than the Langmuir model. Pseudo-first order and pseudo-second order models were used to study the adsorption kinetics. The results showed that the pseudo-second order model was more reliable than the pseudo-first order model in the study of the adsorption process of Cr(VI).

Acknowledgments This work was supported by National Natural Science Foundation of China (No. 21706127) and Natural Science Foundation of Jiangsu Province (BK20140939). The authors also gratefully appreciate the support from National/Jiangsu Students Innovation and Entrepreneurship Training Program (Nos. 201710291015, 201710291016, 201710291016Z, 201710291017Z). The financial support from Nanjing Tech University (free topics on International Cooperation Training Project) was also gratefully appreciated.

References

Ahmad M, Ahmed S, Swami BL, Ikram S (2015) Preparation and characterization of antibacterial thiosemicarbazide chitosan as efficient Cu(II) adsorbent. Carbohydr Polym 132:164–172

Ahmad M, Manzoor K, Venkatachalam P, Ikram S (2016) Kinetic and thermodynamic evaluation of adsorption of Cu(II) by thiosemicarbazide chitosan. Int J Biol Macromol 92:910–919

Ahmad M, Manzoor K, Chaudhuri RR, Ikram S (2017a) Thiocarbohydrazide cross-linked oxidized chitosan and poly(-vinyl alcohol): a green framework as efficient Cu(II), Pb(II), and Hg(II) adsorbent. J Chem Eng Data 62(7):2044–2055

Ahmad M, Manzoor K, Ikram S (2017b) Versatile nature of hetero-chitosan based derivatives as biodegradable adsorbent for heavy metal ions; a review. Int J Biol Macromol 105:190–203

Azarova YA, Pestov AV, Bratskaya SY (2016) Application of chitosan and its derivatives for solid-phase extraction of metal and metalloid ions: a mini-review. Cellulose 23(4):2273–2289

Bano I, Arshad M, Yasin T, Ghauri MA, Younus M (2017) Chitosan: a potential biopolymer for wound management. Int J Biol Macromol 102:380–383

Barrera-Diaz CE, Lugo-Lugo V, Bilyeu B (2012) A review of chemical, electrochemical and biological methods for aqueous Cr(VI) reduction. J Hazard Mater 223–224:1–12

Bhatt R, Sreedhar B, Padmaja P (2015) Adsorption of chromium from aqueous solutions using crosslinked chitosan-diethylenetriaminepentaacetic acid. Int J Biol Macromol 74:458–466

Bhatt R, Sreedhar B, Padmaja P (2017) Chitosan supramolecularly cross linked with trimesic acid-facile synthesis, characterization and evaluation of adsorption potential for chromium(VI). Int J Biol Macromol 104:1254–1266

Camarada MB, Zuniga M, Alzate-Morales J, Santos LS (2014) Computational study of the complexation of metals ions with poly(amidoamine) PAMAM G0 dendrimers. Chem Phys Lett 616–617:171–177

Chauhan D, Jaiswal M, Sankararamakrishnan N (2012) Removal of cadmium and hexavalent chromium from

electroplating waste water using thiocarbamoyl chitosan. Carbohydr Polym 88(2):670–675

Chen DM, Li W, Wu YR, Zhu Q, Lu ZJ, Du GX (2013) Preparation and characterization of chitosan/montmorillonite magnetic microspheres and its application for the removal of Cr(VI). Chem Eng J 221:8–15

Chen XM, Zhang WG, Luo XL, Zhao F, Li YX, Li RH, Li ZH (2017) Efficient removal and environmentally benign detoxification of Cr(VI) in aqueous solutions by Zr(IV) cross-linking chitosan magnetic microspheres. Chemosphere 185:991–1000

Debnath S, Maity A, Pillay K (2014) Magnetic chitosan-GO nanocomposite: synthesis, characterization and batch adsorber design for Cr(VI) removal. J Environ Chem Eng 2:963–973

Gandhi MR, Meenakshi S (2013) Preparation of amino terminated polyamidoamine functionalized chitosan beads and its Cr(VI) uptake studies. Carbohydr Polym 91(2):631–637

He GH, Zhu C, Ye SG, Cai WQ, Yin YH, Zheng H, Yi Y (2016) Preparation and properties of novel hydrogel based on chitosan modified by poly(amidoamine) dendrimer. Int J Biol Macromol 91:828–837

Hu JJ, Xu TW, Cheng YY (2012) NMR insights into dendrimer-based host-guest systems. Chem Rev 112(7):3856–3891

Huang JN, Cao YH, Shao Q, Peng XF, Guo ZH (2017) Magnetic nanocarbon adsorbents with enhanced hexavalent chromium removal: morphology dependence of fibrillar vs particulate structures. Ind Eng Chem Res 56(38):10689–10701

Jiang LH, Liu SB, Liu YG, Zeng GM, Guo YM, Yin YC, Cai XX, Zhou L, Tan XF, Huang XX (2017) Enhanced adsorption of hexavalent chromium by a biochar derived from ramie biomass (*Boehmeria nivea* (L.) Gaud.) modified with beta-cyclodextrin/poly(L-glutamic acid). Environ Sci Pollut Res Int 24(30):23528–23537

Jin W, Du H, Zheng SL, Zhang Y (2016) Electrochemical processes for the environmental remediation of toxic Cr(VI): a review. Electrochim Acta 191:1044–1055

Kimbrough DE, Cohen Y, Winer AM, Creelman L, Mabuni C (1999) A critical assessment of chromium in the environment. Crit Rev Environ Sci Technol 29(1):1–46

Kousalya GN, Gandhi MR, Meenakshi S (2010) Sorption of chromium(VI) using modified forms of chitosan beads. Int J Biol Macromol 47(2):308–315

Lee SK, Lalchhingpuii L, Tiwari D (2016) Synthesis of functionalized biomaterials and its application in the efficient remediation of aquatic environment contaminated with Cr(VI). Chem Eng J 296:35–44

Li L, Li YX, Cao LX, Yang CF (2015) Enhanced chromium (VI) adsorption using nanosized chitosan fibers tailored by electrospinning. Carbohydr Polym 125:206–213

Li R, An QD, Xiao ZY, Zhai B, Zhai SR, Shi Z (2017) Preparation of PEI/CS aerogel beads with a high density of reactive sites for efficient Cr(VI) sorption: batch and column studies. RSC Adv 7(64):40227–40236

López-Cabaña ZE, Valdes O, Vergara CE, Camarada MB, Nachtigall FM, González-Nilo FD, Santos LS (2015) Photophysical studies of the interactions of poly(amidoamine) generation zero (PAMAM G0) with copper and zinc ions. J Lumin 164:23–30

Lyu HH, Tang JC, Huang Y, Gai LS, Zeng EY, Liber K, Gong YY (2017) Removal of hexavalent chromium from aqueous solutions by a novel biochar supported nanoscale iron sulfide composite. Chem Eng J 322:516–524

Ma F, Qu RJ, Sun CM, Wang CH, Ji CN, Zhang Y, Yin P (2009) Adsorption behaviors of Hg(II) on chitosan functionalized by amino-terminated hyperbranched polyamidoamine polymers. J Hazard Mater 172(2–3):792–801

Ma ZX, Garrido-Maestu A, Jeong KC (2017) Application, mode of action, and in vivo activity of chitosan and its micro- and nanoparticles as antimicrobial agents: a review. Carbohydr Polym 176:257–265

Pradhan D, Sukla LB, Sawyer M, Rahman PKSM (2017) Recent bioreduction of hexavalent chromium in wastewater treatment: a review. J Ind Eng Chem 55:1–20

Preethi J, Prabhu SM, Meenakshi S (2017) Effective adsorption of hexavalent chromium using biopolymer assisted oxyhydroxide materials from aqueous solution. React Funct Polym 117:16–24

Sakulthaew C, Chokejaroenrat C, Poapolathep A, Satapanajaru T, Poapolathep S (2017) Hexavalent chromium adsorption from aqueous solution using carbon nano-onions (CNOs). Chemosphere 184:1168–1174

Salehi E, Daraei P, Shamsabadi AA (2016) A review on chitosan-based adsorptive membranes. Carbohydr Polym 152:419–432

Sankararamakrishnan N, Sanghi R (2006) Preparation and characterization of a novel xanthated chitosan. Carbohydr Polym 66(2):160–167

Shen CS, Chen H, Wu SS, Wen YZ, Li LN, Jiang Z, Li MC, Liu WP (2013) Highly efficient detoxification of Cr(VI) by chitosan-Fe(III) complex: process and mechanism studies. J Hazard Mater 244–245:689–697

Thinh NN, Hanh PTB, le Ha TT, le Anh N, Hoang TV, Hoang VD, le Dang H, Khoi NV, Lam TD (2013) Magnetic chitosan nanoparticles for removal of Cr(VI) from aqueous solution. Mater Sci Eng C Mater Biol Appl 33(3):1214–1218

Vendruscolo F, da Rocha Ferreira GL, Antoniosi Filho NR (2017) Biosorption of hexavalent chromium by microorganisms. Int Biodeterior Biodegradation 119:87–95

Vieira RS, Oliveira MLM, Guibal E, Rodríguez-Castellón E, Beppu MM (2011) Copper, mercury and chromium adsorption on natural and crosslinked chitosan films: an XPS investigation of mechanism. Colloids Surf A 374(1–3):108–114

Wang GW, Zhuang LH, Sun J, Zheng CL (2014) Salt-free dyeing of ramie fabric with an amino-terminated hyperbranched polymer. Cellulose 21(5):3725–3736

Wang GW, Chen B, Zhuang LH, Yun K, Guo JR, Wang Y, Xu B (2015) Dyeing performances of ramie fabrics modified with an amino-terminated aliphatic hyperbranched polymer. Cellulose 22(2):1401–1414

Wang JH, Wang L, Yu HJ, Abdin Z, Chen YS, Chen Q, Zhou WD, Zhang HT, Chen X (2016) Recent progress on synthesis, property and application of modified chitosan: an overview. Int J Biol Macromol 88:333–344

Wang HX, Qian J, Ding FY (2017) Recent advances in engineered chitosan-based nanogels for biomedical applications. J Mater Chem B 5(34):6986–7007

Wen Y, Tang ZR, Chen Y, Gu YX (2011) Adsorption of Cr(VI) from aqueous solutions using chitosan-coated fly ash composite as biosorbent. Chem Eng J 175:110–116

Wu YH, Cha LG, Fan YA, Fang P, Ming Z, Sha HT (2017) Activated biochar prepared by pomelo peel using H3PO4 for the adsorption of hexavalent chromium: performance and mechanism. Water Air Soil Pollut 228:405

Xie BH, Shan C, Xu Z, Li XC, Zhang XL, Chen JJ, Pan BC (2017) One-step removal of Cr(VI) at alkaline pH by UV/sulfite process: reduction to Cr(III) and in situ Cr(III) precipitation. Chem Eng J 308:791–797

Xu B, Li QP, Zhuang LH, Wang Q, Li C, Wang GW, Xie FW, Halley PJ (2016) Dissolution and regeneration behavior of chitosan in 3-methyl-1-(ethylacetyl)imidazolium chloride. Fibers Polym 17(11):1741–1748

Zarghami Z, Akbari A, Latifi AM, Amani MA (2016) Design of a new integrated chitosan-PAMAM dendrimer biosorbent for heavy metals removing and study of its adsorption kinetics and thermodynamics. Bioresour Technol 205:230–238

Zhang LF, Xia W, Teng B, Liu X, Zhang WQ (2013) Zirconium cross-linked chitosan composite: preparation, characterization and application in adsorption of Cr(VI). Chem Eng J 229:1–8

Zhang L, Zeng YX, Cheng ZJ (2016) Removal of heavy metal ions using chitosan and modified chitosan: a review. J Mol Liq 214:175–191

Zheng YC, Li SP, Weng ZL, Gao C (2015) Hyperbranched polymers: advances from synthesis to applications. Chem Soc Rev 44(12):4091–4130

Zhou LL, Zhang GL, Wang M, Wang DF, Cai DQ, Wu ZY (2018) Efficient removal of hexavalent chromium from water and soil using magnetic ceramsite coated by functionalized nano carbon spheres. Chem Eng J 334:400–409

Zimmermann AC, Mecabo A, Fagundes T, Rodrigues CA (2010) Adsorption of Cr(VI) using Fe-crosslinked chitosan complex (Ch-Fe). J Hazard Mater 179(1–3):192–196